AJNR

A Technique for Improved Quantitative Characterization of Intracranial Aneurysms

Christof Karmonik, Anil Arat, Goetz Benndorf, Sergin Akpek, Richard Klucznik, Michel E. Mawad and Charles M. Strother

AJNR Am J Neuroradiol 2004, 25 (7) 1158-1161
http://www.ajnr.org/content/25/7/1158

AJNR Am J Neuroradiol 25:1158–1161, August 2004

A Technique for Improved Quantitative Characterization of Intracranial Aneurysms

Christof Karmonik, Anil Arat, Goetz Benndorf, Sergin Akpek, Richard Klucznik, Michel E. Mawad, and Charles M. Strother

Summary: 3D digital subtraction angiograms of two intracranial aneurysms were imported to a workstation for reconstruction and postprocessing into a format allowing delineation of 1) the extent to which the diameter of the parent artery is incorporated into the aneurysm ostium (percentage of parent artery involvement or neck angle) and 2) the aneurysm volume and surface area. For clear visualization, 3D surface-rendered objects of the reconstructed artery, neck angle, and aneurysm were created.

Aneurysm morphology influences both the incidence of bleeding and the outcome of endovascular therapy (1, 2). Although 3D digital subtraction angiographic (DSA) techniques are widely used to define some features of aneurysm morphology (eg, maximum dimensions, neck size, and relationships to parent artery and adjacent branches), they do not provide a rapid means for defining other features, such as the geometry of the ostium (face), surface area, or volume. We describe a technique based on 3D DSA data that we believe will be helpful for more complete quantitative classification of aneurysms.

Description of the Technique

Image Preprocessing

3D DSA images were retrospectively obtained from imaging studies done as part of diagnostic evaluations of intracranial aneurysms. Data were obtained with C-arm systems (Axiom Artis; Siemens, Medical Systems, Erlangen, Germany) by using commercially available hardware and software. Image data were transferred to a personal computer for further off-line processing by using workstation software (eFilm; Merge, eFilm, Toronto, Canada). 3D maximum intensity projection was used to define the orientation of the aneurysm and the parent artery. Next, a contiguous set of 2D cross-sections (0.1-mm thickness oriented approximately perpendicular to the axis of the parent artery and encompassing the entire aneurysm) was obtained by using the multiplanar image reconstruction feature of the eFilm software. These were then imported into ImageJ (ImageJ, 2003; National Institutes of Health, Bethesda, MD) as an image stack for further processing with JAVA plug-ins developed in-house.

To obtain a sharp boundary between the vascular lumen and the surrounding tissue, images were manually windowed. For each cross-section, the image pixels that constituted the lumen boundary were extracted by using an automatic tracing tool. This boundary point set was ordered and stored in a circular buffer.

Reconstruction of the Parent Artery

The parent artery was then reconstructed by the following procedure. For each cross-section that preceded or succeeded the aneurysm ostium in the image stack, the radial center of the artery was determined as the center of mass of the boundary points of the arterial lumen. The arterial radius was then calculated as the average distance between the boundary points and this center.

For a cross-section containing the aneurysm ostium, a user-defined region of interest included only boundary points belonging to the normal arterial wall. Boundary points outside this region of interest were ignored. This dataset was further reduced by discarding those points exceeding a certain radial distance from the arterial center determined in the *preceding* cross-section. A single value decomposition algorithm (3) was then used to find the arterial center for this section. The radius of the artery was determined as the average distance of this center point to the reduced set of boundary points. Iteratively applied to all remaining cross-sections, this algorithm determined the center and radius of the artery along the lateral extension of the aneurysm ostium.

Determination of the Neck Angle of the Aneurysm

After the center and the radius of the parent artery were computed, the search algorithm traversed the boundary points in an ordered fashion and tested to see if the distance between a point and the center of the artery exceeded a certain threshold value. The identification of such a location marked one extent of the aneurysm ostium. The algorithm continued to traverse the boundary points until it encountered a distance value lower than the threshold value. This location defined the other extent of the ostium. After the search algorithm successfully ended, it had identified the first and the last aneurysm boundary point. The difference in the angles of these two boundary points was defined as the neck angle (percentage parent artery involvement by the ostium) of the aneurysm.

Derivation of Topologic Parameters

After the parent artery was reconstructed and the neck angle of the aneurysm determined, several topologic parameters could then be easily derived. These were the area of the aneurysm ostium, the dome height in each cross-section, the maximum dome height, the location of the maximum neck angle (percentage of the parent artery incorporated by the

Received December 3, 2003; accepted after revision February 20, 2004.

From the Department of Radiology, Baylor College of Medicine (C.K., M.E.M., S.A., G.B., C.M.S.), Department of Radiology, the Methodist Hospital (A.A., M.E.M., R.K., C.M.S.), Houston, TX.

Address reprint requests to Christof Karmonik, Department of Radiology, Baylor College of Medicine, M 214, 6565 Fannin, Houston, TX 77030.

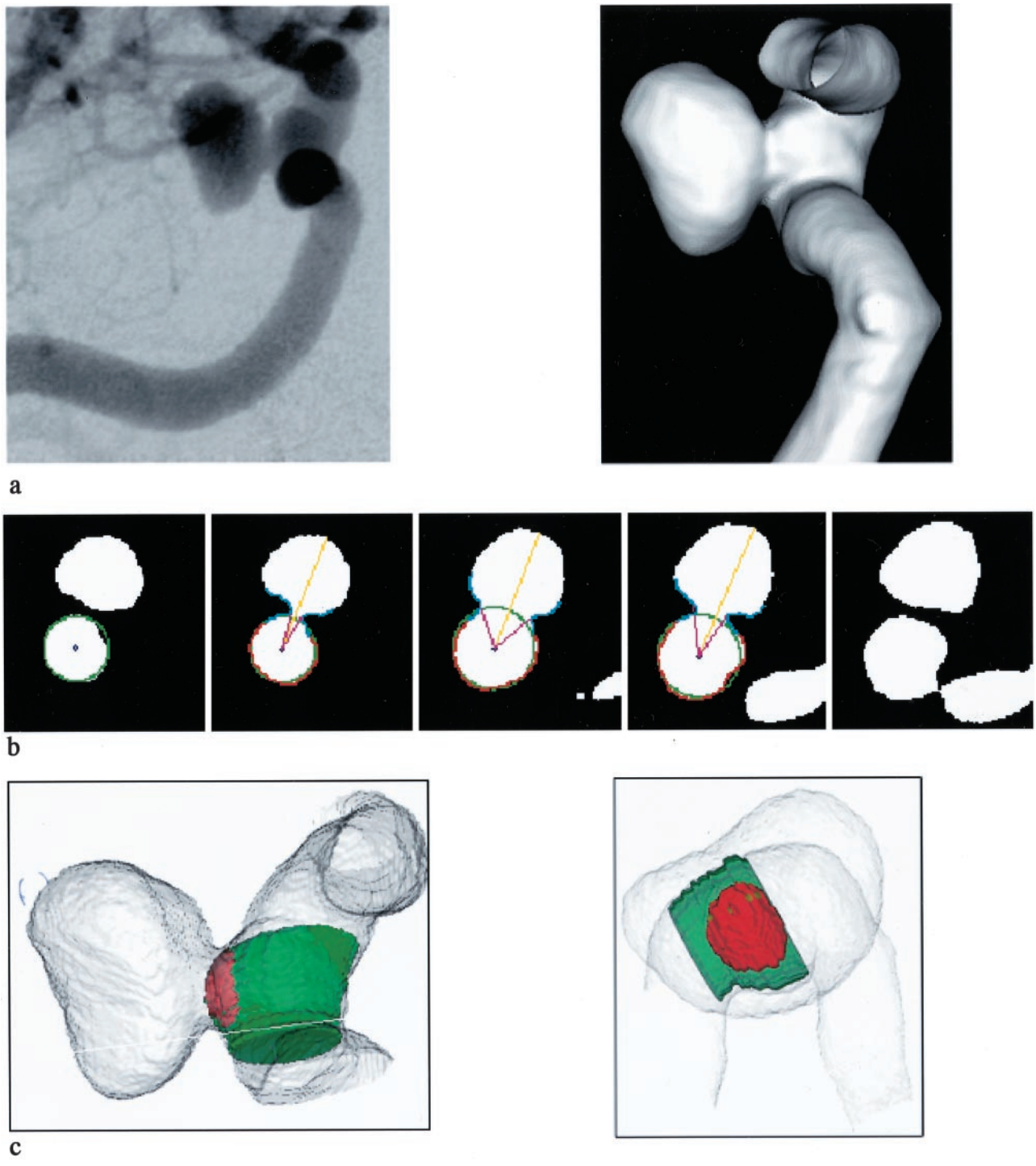

FIG 1. Case 1. *Top*, 2D DSA image (anteroposterior projection) and 3D DSA surface reconstruction from a right ICA angiogram showing a large paraopthalmic aneurysm. *Middle*, Results produced by the algorithm for selected cross-sections perpendicular to the axis of the parent artery shows the reconstructed vessel (*green*), neck angle (*purple*), and dome height (*yellow*, from *green* to top). Boundary points used to calculate the vessel parameters are *red*. *Bottom*, 3D surface rendering of the reconstructed artery (*green*) and ostium surface area (*red*) superimposed on the original 3D DSA data (*gray*). In *top* and *bottom* images, *left* is the lateral view; *right*, view from top.

ostium), the ostium length, the aneurysm surface area, and the aneurysm volume.

3D Visualization of the Aneurysm and the Reconstructed Artery

For easier visualization of the results, the visualization toolkit (Kitware, Clifton Park, NY) (4) was used to create 3D surface-rendered objects of the thresholded 3D DSA data, the reconstructed artery, the ostium and the aneurysm.

Using this technique, we assessed two aneurysms: one (case 1, Fig 1) could be considered to represent an ideal example, while the second (case 2, Fig 2) highlighted the methodologic limitations of the technique. Image *A* in each figure displays a 2D projection image and the 3D DSA surface reconstruction

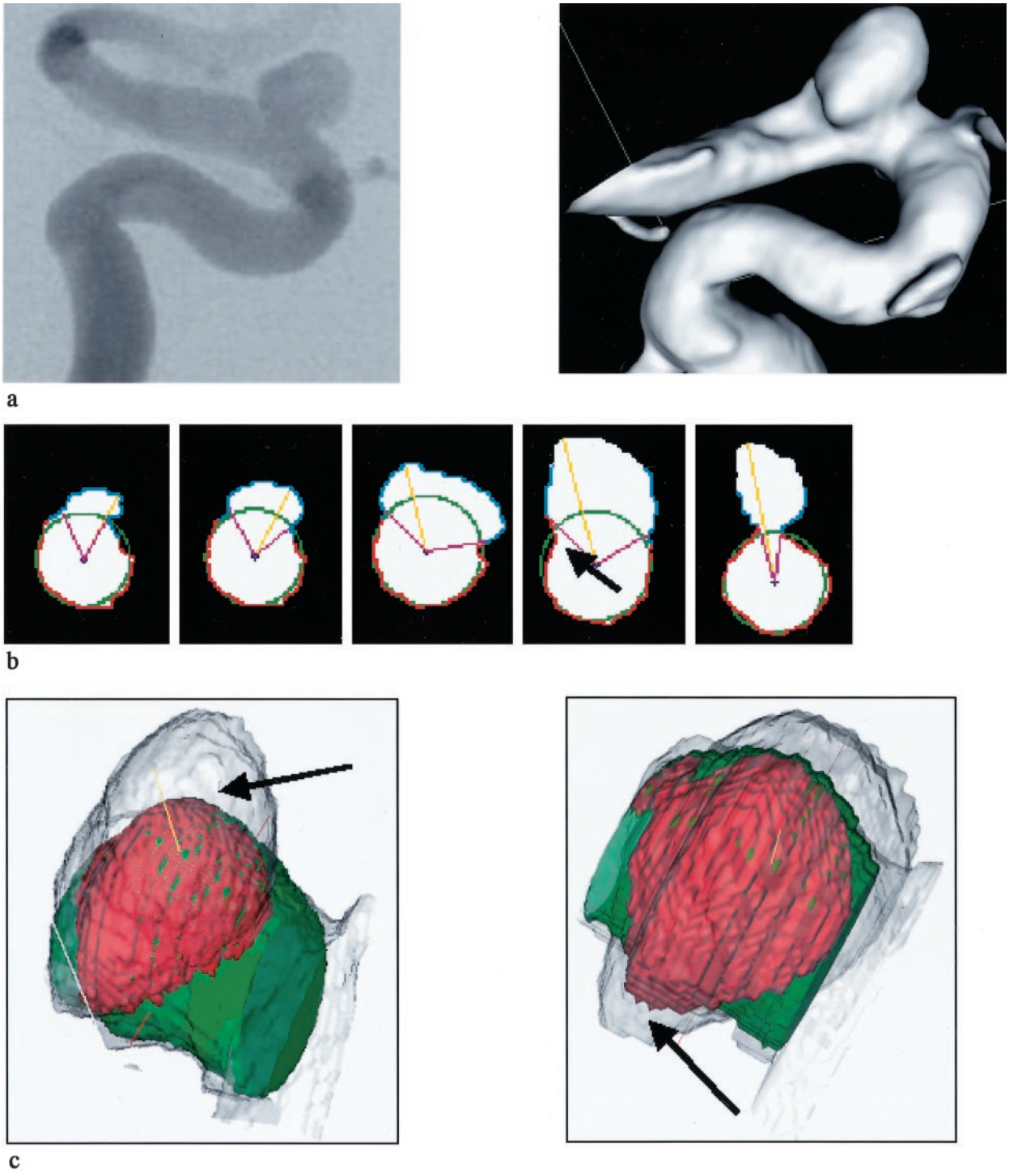

FIG 2. Case 2. *Top*, 2D DSA image (lateral projection) and 3D DSA surface reconstruction from a right ICA angiogram showing a small supraclinoid ICA aneurysm. *Middle*, Results produced by the algorithm for selected cross-sections perpendicular to the axis of the parent artery shows the reconstructed vessel (*green*), neck angle (*purple*), and dome height (*yellow*, from *green* to top). Boundary points used to calculate the vessel parameters are *red*. The reconstructed vessel exceeds the boundary of the parent artery in cross-section 4 (*arrow*). *Bottom*, 3D surface rendering of the reconstructed artery (*green*) and ostium surface area (*red*) superimposed on the original 3D DSA data (*gray*) reveals the increase of the radius of the reconstructed artery along the aneurysm ostium (*arrows*). In *top* and *bottom* images, *left* is the lateral view; *right*, view from top.

for each case. Image *B* shows the reconstructed artery and the neck angle of the aneurysm on selected cross-sections, and image *C* shows the 3D surface-rendered objects of the reconstructed artery and the aneurysm neck area overlaid onto the original 3D DSA data. The Table lists the values for the topologic parameters.

Discussion

Aneurysm morphology has been shown to influence both the incidence of bleeding and the results of endovascular therapy (1, 2). Although commercially available 3D DSA techniques allow rapid and clear

Values for topologic parameters

Parameter	Case 1	Case 2
Maximum neck angle, °	71	139
Parent artery involvement, %	20	39
Ostium length, mm	2.5	4.8
Aneurysm surface area, mm^2	143	64
Aneurysm volume, mm^3	148	56
Dome-to-neck ratio	1.4	1.0
Aneurysm surface-to-ostium area ratio	18.8	2.5

depiction of some anatomic features of intracranial aneurysms (eg, maximum dimensions, neck width, and relationships to parent artery and adjacent branches), they do not provide the ability to fully define and quantify other features, such as the extent to which the ostium involves the diameter of the parent artery, the volume, or the surface area.

Why is it of possible importance to provide this information? The concept of an aneurysm neck was originally derived from open surgical techniques. Most recent endovascular literature still uses this concept and divides aneurysms into those with narrow necks and those with wide necks, arbitrarily setting the measurement that distinguishes the two categories as being 4 mm. A more meaningful concept for endovascular therapy (and perhaps for the determination of an aneurysm's natural history as well) is that of the aneurysm ostium, a feature that defines the extent of the parent arterial diameter involved by an aneurysm. To our knowledge, there is no systematic information regarding this feature of intracranial aneurysms; however, it seems certain that some small aneurysms with a narrow neck (now thought to be ideal aneurysms for endovascular treatment) have an ostium that is slitlike (ie, they involve only a small percentage of the parent-artery diameter), whereas others have an ostium that is oval or elliptical (ie, they involve a much larger percentage of the parent-artery diameter). The ease of endovascular treatment and the incidence of recurrence following treatment of these two aneurysms are likely different. Currently available 3D DSA techniques do not provide a means to derive this information.

Accurate measurement of aneurysm volume and surface area are not now of proved value. This information may be needed for the safe and effective use of materials that will soon be available for clinical application. These include liquid materials with physical characteristics that change once they are placed into an aneurysm and coils that combine a metal or polymer with a radioactive source or pharmaceutical agent. Volume measurements will be needed to determine the amount of liquid material needed for complete treatment. Similarly, surface-area measurements will be needed to calculate radiation or drug dosages.

Several limitations in our technique are evident. First, to achieve good reconstruction of the parent artery, the reduced set of boundary points for each cross-section must contain points sufficient to define the radius and the curvature of the artery. This is the case for all cross-sections of case 1 (Fig 1, *middle*). However, for case 2, deviations from the idealized circular shape of the parent artery are noticeable, as this requirement was not met (Fig 2, *middle*). Because the algorithm provides the best fit of the DSA data to a circular shape of an ideal artery, any variation from such a shape leads to some error. Because of this, the arterial radius (*green circle* in Fig 2, *middle*) was slightly overestimated in case 2. Errors of this nature can also arise when it is not possible to create cross-sections sufficiently perpendicular to the long axis of the parent artery (eg, in cases in which the artery exhibits a strong curvature along the aneurysm neck). Also, if an aneurysm does not have a sidewall configuration or if vessels branch from the parent artery at the location of the aneurysm neck, the circular shape of the artery may be distorted. In such instances, manual editing of the DSA data is necessary before the algorithm is applied.

If the arterial radius is not well defined and if there is no clear distinction between the aneurysm dome and the aneurysm neck, the definition of the aneurysm neck angle, becomes ambiguous (cross-sections 3 and 4 of Fig 2, *middle*). Increased user interaction and visual inspection is then necessary to obtain acceptable results.

Errors in determining the arterial radius, and therefore in the maximum neck angle, will propagate to the topologic parameters that are derived from them. These errors are linear. Those that would occur in determining surface area or volume are more difficult to assess, as they may depend not only on the cross-sections along the aneurysm ostium but also on other cross-sections as well (eg, in the instance of a dumbbell-shaped aneurysm).

Therefore, it is necessary for the user to visually inspect the result so that these limitations are recognized. The technique of 3D surface-rendering visualization is favorable for this task, as it allows the simultaneous display of the result for all cross-sections. Here, the results for case 1 were seen to be adequate (Fig 1, *bottom*), whereas the increase of the radius of the reconstructed artery along the aneurysm ostium that is discernable in case 2 (*arrows* in Fig 2, *bottom*) should alert the user to review for a possible error in the analysis.

References

1. Wiebers DO, Whisnant JP, Huston J III, et al. **Unruptured intracranial aneurysms: natural history, clinical outcome, and risk of surgical and endovascular treatment.** *Lancet* 2003;362:103–110
2. Brilstra EH, Rinkel GJE, van der Graaf Y, van Rooij WJJ, Algra A. **Treatment of intracranial aneurysms by embolization with coils: a systematic review.** *Stroke* 1999;30:470–476
3. Press WH, Teukolsky SA, Vetterling WT, Flannery BP. **Solution of linear algebraic equations**. In: *Numerical Recipes in C.* New York: Cambridge University Press; 1992:59–70
4. Lorensen WE, Cline HE. **Marching cubes: a high resolution 3D surface construction algorithm.** *Comput Graphics* 1987;21:163–169